Supporting Information

Water Oxidation Electrocatalyzed by An Efficient $Mn_3O_4/CoSe_2$ Nanocomposite

*Min-Rui Gao, Yun-Fei Xu, Jun Jiang, Ya-Rong Zheng, and Shu-Hong Yu**

Experimental Section

All chemicals are of analytical grade and were used as received without further purification.

Synthesis of $CoSe_2$/DETA Nanobelts (NBs) and their hybrid with Mn_3O_4 nanoparticles (NPs). Lamellar mesostructured $CoSe_2$/DETA NBs were first synthesized as described in ref. S1. For the preparation of $Mn_3O_4/CoSe_2$ hybrid, 50 mg as-prepared $CoSe_2$/DETA NBs was dispersed in 30 ml triethylene glycol (TREG) and sonicated for about 10 min under ambient conditions. After that, 0.3 mmol manganese (III) 2,4-pentanedionate ($Mn(acac)_3$, Alfa Aesar, 99%) was added into the suspension. After vigorous mechanical stirring for about 5 min to dissolve completely, the mixture was slowly heated to reflux to 278 ^oC at a rate of 3 $^oC\ min^{-1}$ and kept at reflux for 1 h under mechanical stirring and nitrogen protection. After cooling to room temperature naturally, the solution was diluted with 40 ml ethanol and ethyl acetate (volume ratio = 1 : 3). The final sample was collected by centrifugation, then washed several times by distilled water and ethanol to remove excess TREG, and vacuum dried at 60 ^oC for 6 h.

To prepare over-loaded-$Mn_3O_4/CoSe_2$ and over-grew-$Mn_3O_4/CoSe_2$hybrids, the synthetic procedures are the same with the procedure for $Mn_3O_4/CoSe_2$ hybrid. The only differences are that the dosage of $Mn(acac)_3$ were increased to 0.6 mmol for the over-loaded-$Mn_3O_4/CoSe_2$ hybrid, and the reaction temperature was increased to 290 ^oC for the over-grew-$Mn_3O_4/CoSe_2$ hybrid, respectively.

Synthesis of free Mn_3O_4 nanorods (NRs) and free Mn_3O_4 NPs. The synthetic procedure for free Mn_3O_4 NRs is the same with the procedure for $Mn_3O_4/CoSe_2$ hybrid. The only difference is that no $CoSe_2$/DETA NBs were added during the synthesis.

To assess the OER activity of free Mn_3O_4 NPs, we prepared two kinds of Mn_3O_4 NPs based on the procedures from ref. S2 and ref. S3, respectively, and then checked their OER properties. From the literatures, pure tetragonal Mn_3O_4 NPs (JCPDS 24-0734) can be successfully obtained (see Figure S3a, b; Figure S3d, e). It should be noticed that the average size of Mn_3O_4 NPs we synthesized is bigger than the literatures, but this may have no effect on the qualitative assessment of the OER activity of Mn_3O_4 NPs.

Characterization. The samples were characterized by different analytic techniques. X-Ray powder diffraction (XRD) was carried out on a Rigaku D/max-rA X-ray diffractometer with Cu Ka radiation (λ = 1.54178 Å), Scanning electron microscope (SEM, JSM-6700F) was applied to investigate the size and morphology. TEM images, HRTEM images, selected-area electron diffraction (SAED), and an Energy-disperse X-ray spectrum (EDX) were taken with a JEOJ-2010 transmission electron microscope with an acceleration voltage of 200 kV. The Fourier transform infrared (FT-IR) spectra were measured on a Bruker Vector-22 FT-IR spectrometer at room temperature. The X-ray photoelectron spectra (XPS) were recorded on an ESCALab MKII X-ray photo-electron spectrometer using Mg Ka radiation exciting source. The powder sample was attached to carbon tape and was set in the XPS chamber. Calibration of binding energy was carried out by setting binding energy of C1s peak to 284.5 eV. The X-ray absorption near edge structure (XANES) measurements were performed in transmission mode at U7C XAFS station in NSRL (National Synchrotron Radiation Laboratory, Hefei, P. R. China).

Electrocatalytic Study. Electrochemical measurements were performed at room temperature using a rotating disk working electrode made of glassy carbon (PINE, 5 mm diameter, 0.196 cm^2) connected to a Multipotentiostat (IM6ex, ZAHNER elektrik, Germany). The glassy carbon electrode was polished to a mirror finish (No. 40-6365-006, Gamma Micropolish Alumina, Buehler; No.40-7212, Microcloth,

Buehler) and thoroughly cleaned before use. Pt wire and Ag/AgCl (PINE, 4 M KCl) were used as counter and reference electrodes, respectively. The potentials reported in our work were vs. Ag/AgCl or vs. the reversible hydrogen electrode (RHE) through RHE calibration described below.

The preparation method of the working electrodes containing investigated catalysts can be found as follows. In short, 5 mg of catalyst powder was dispersed in 1 ml of 3:1 v/v water/isopropanol mixed solvent with 40 μl of Nafion solution (5 wt%, Sigma-Aldrich), then the mixture was ultrasonicated for at least 30 min to generate a homogeneous ink. Next, 8 μl of the dispersion was transferred onto the galssy carbon disk, leading to the catalyst loading ~0.2 mg cm^{-2}. Finally, the as-prepared catalyst film was dried at room temperature. For comparison, bare glassy carbon electrode which has been polished and cleaned was also dried for electrochemical measurement.

Before the electrochemical measurement, the electrolyte (0.1 M KOH, pH ~13) was degassed by bubbling oxygen for 30 min. The polarization curves were obtained by sweeping the potential from 0 to 0.8 V vs. Ag/AgCl at room temperature and 1600 rpm, with a sweep rate of 5 mV s^{-1}. The cyclic voltammetry (CV) curves were obtained by sweeping the potential from -0.9 to 1 V vs. Ag/AgCl at room temperature and 1600 rpm. All the data were recorded after applying a number of potential sweeps until which were stable.

The accelerated stability tests were performed in O_2-saturated 0.1 M KOH at room temperature by potential cycling between 0.3 and 0.8 V vs. Ag/AgCl at a sweep rate of 100 mV/s for given number of cycles. At the end of each cycling, the resulting electrode was used for polarization and CV curves.

RHE calibration. In all measurements, we used Ag/AgCl (PINE, 4 M KCl) as the reference electrode. It was calibrated with respect to RHE. The calibration was performed in the high purity hydrogen saturated electrolyte with a Pt foil as the working electrode. Cyclic voltammetry (CV) was run at a scan rate of 1 mV s^{-1}, and the average of the two potentials at which the current crossed zero was taken to be the thermodynamic potential for the hydrogen electrode reaction. The CV result was shown below:

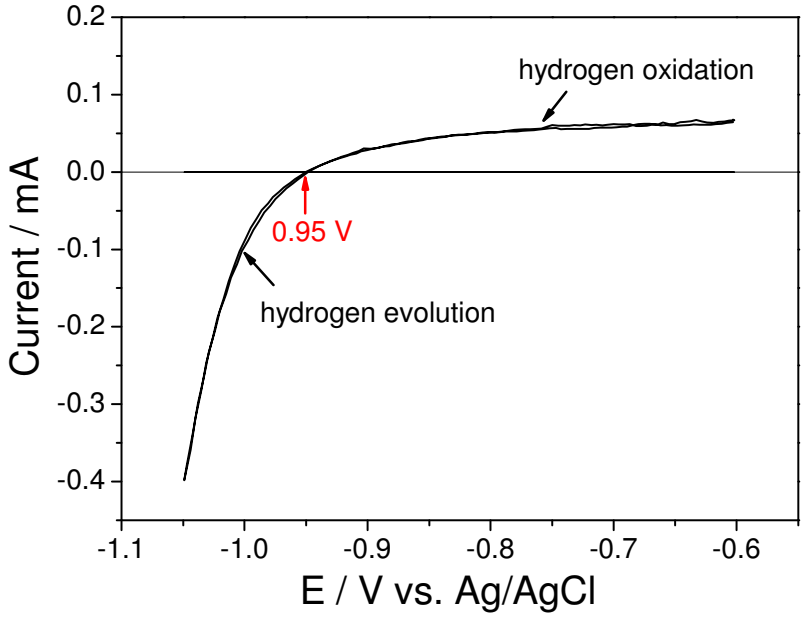

Therefore, in 0.1 M KOH solution, E(RHE) = E(Ag/AgCl) + 0.95 V.

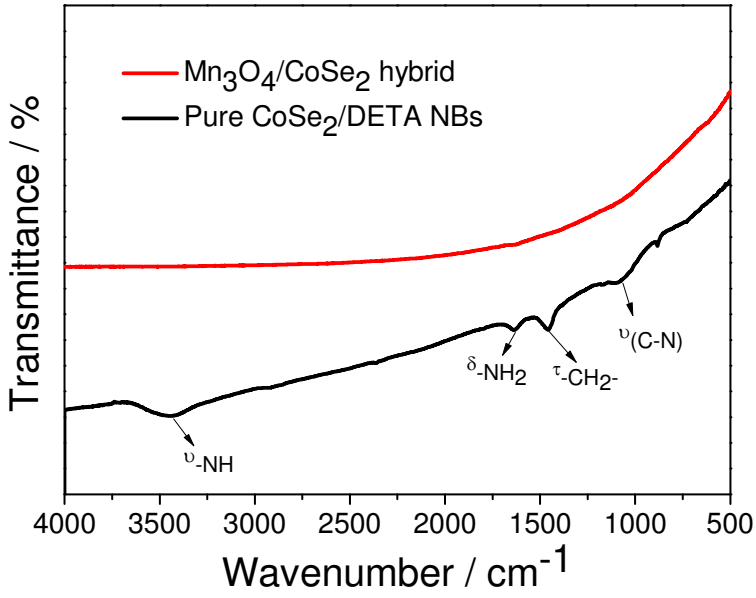

Figure S1. FI-IR spectra of the pure $CoSe_2$/DETA NBs and the constructed $Mn_3O_4/CoSe_2$ hybrid prepared at 278 ^oC for 1 h.

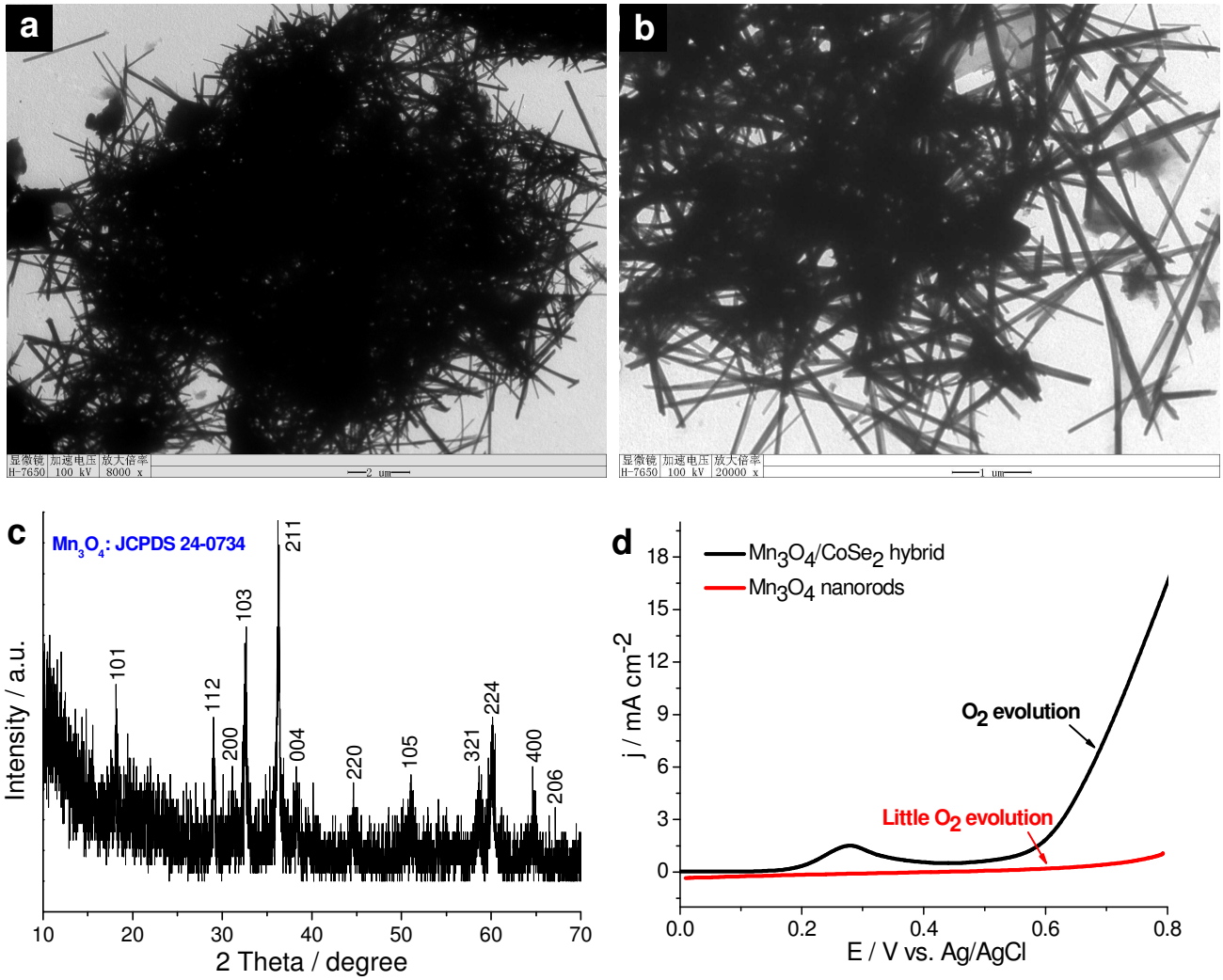

Figure S2. (a, b) TEM images of the morphology of Mn_3O_4 NRs prepared at 278 ^oC for 1 h without any $CoSe_2$/DETA NBs in the synthesis. (c) XRD pattern of the Mn_3O_4 NRs, which displays the tetragonal Mn_3O_4 (JCPDS 24-0734). (d) Polarization curves for OER on free Mn_3O_4 NRs and constructed $Mn_3O_4/CoSe_2$ hybrid, respectively, which shows that Mn_3O_4 NRs are OER-inactive.

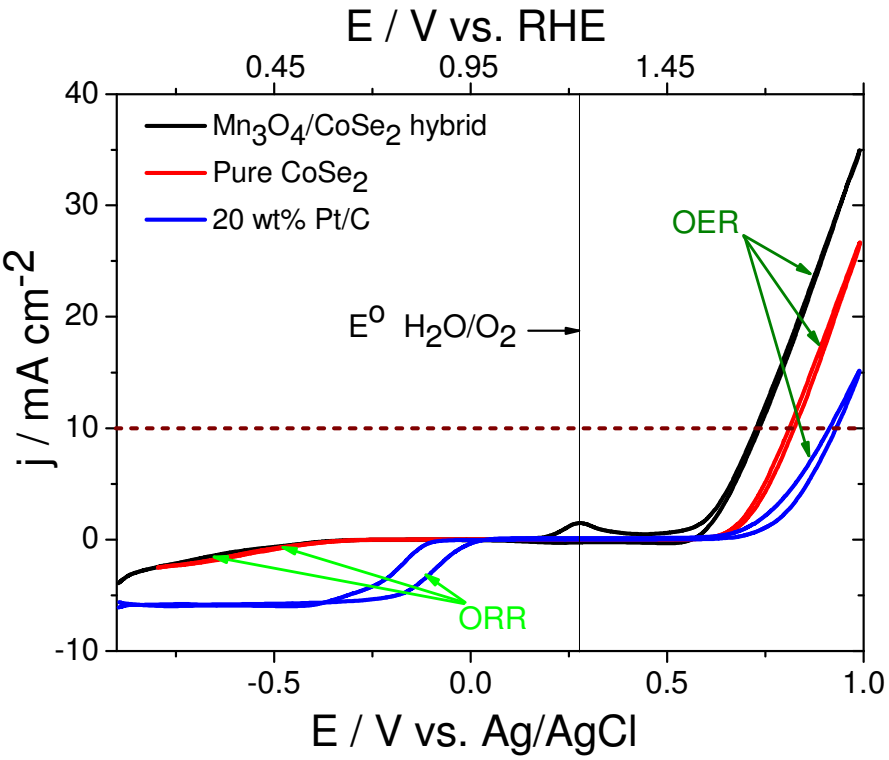

Figure S3. CV curves show the oxygen electrode activities within the oxygen reduction reaction (ORR) and OER potential window of $Mn_3O_4/CoSe_2$ hybrid, pure $CoSe_2$, and commercial Pt/C catalysts in O_2-saturated 0.1 M KOH. Catalyst loading: ~0.2 mg cm^{-2}. Sweep rate: 5 mV s^{-1}.

The ORR activity of $CoSe_2$ nanomaterials in acid medium has been well documented (ref. 2-5). In 0.1 M KOH, $CoSe_2$ and $Mn_3O_4/CoSe_2$ hybrid also showed some ORR activities, which were much lower than that of Pt/C catalyst. However, when the potential was extended to the water oxidation regime, the $Mn_3O_4/CoSe_2$ hybrid and also pure $CoSe_2$ all revealed larger current and earlier onset of catalytic current than that of Pt/C catalyst, indicating such Co-based catalysts bears excellent catalytic activity for OER. Compared with $CoSe_2$, the OER activity of $Mn_3O_4/CoSe_2$ is significantly enhanced, which may arise from synergetic chemical coupling effects between Mn_3O_4 and $CoSe_2$.

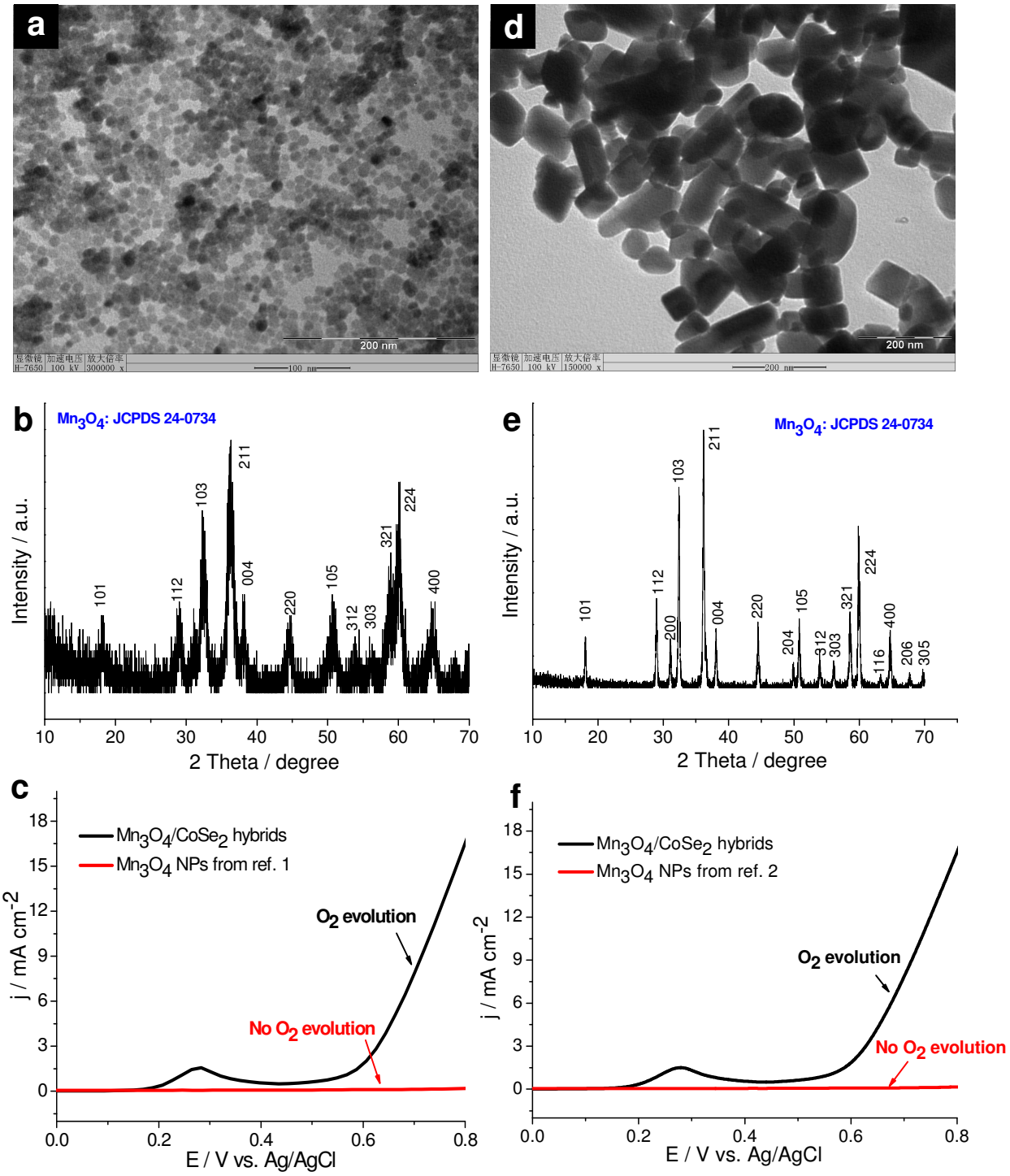

Figure S4. (a, b) TEM image and XRD pattern for the sample prepared based on the **ref. S6**, respectively, which show that the product is tetragonal Mn_3O_4 NPs (JCPDS 24-0734) with an average size of ~9.8 nm. (d, e) TEM and XRD for the sample prepared based on the **ref. S7**, respectively, which show that the product is tetragonal Mn_3O_4 NPs (JCPDS 24-0734) with sizes from tens to hundreds of nanometers. (c, f) Polarization curves for OER on the two kinds of free Mn_3O_4 NPs, and constructed $Mn_3O_4/CoSe_2$ hybrid, respectively, which shows that Mn_3O_4 NPs are OER-inactive.

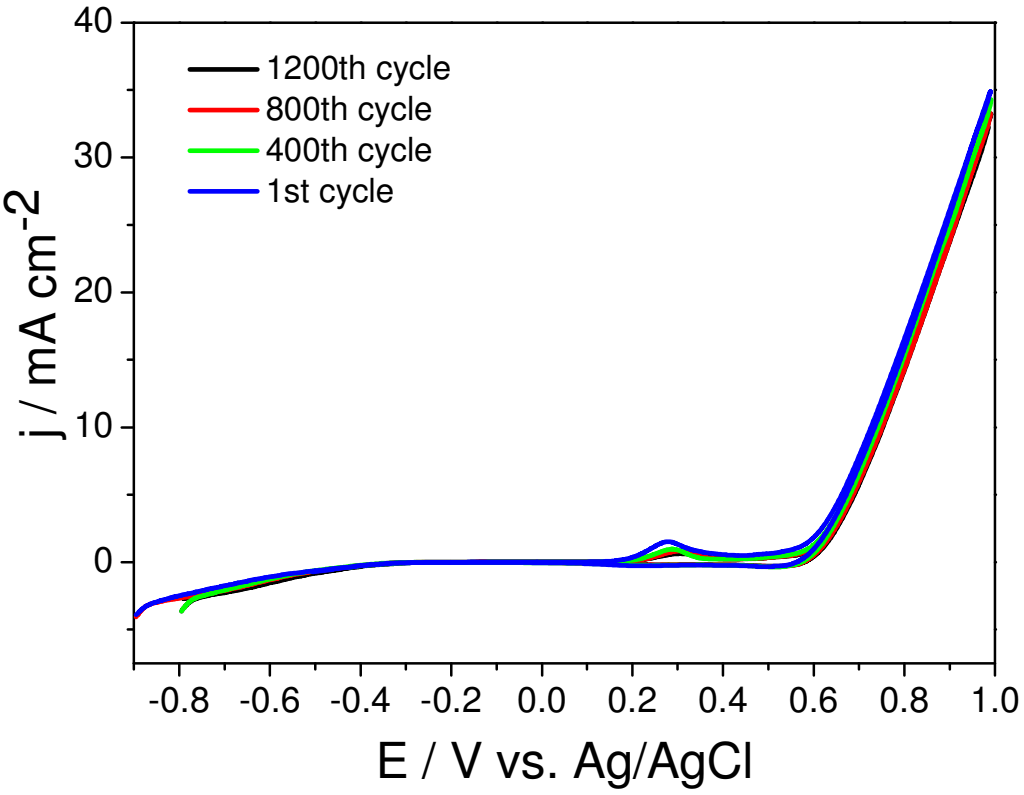

Figure S5. CV curves show the oxygen electrode activities within the oxygen reduction reaction (ORR) and OER potential window of $Mn_3O_4/CoSe_2$ hybrid before and after different cycles of accelerated stability test in O_2-saturated 0.1 M KOH. Catalyst loading: ~0.2 mg cm^{-2}. Sweep rate: 5 mV s^{-1}.

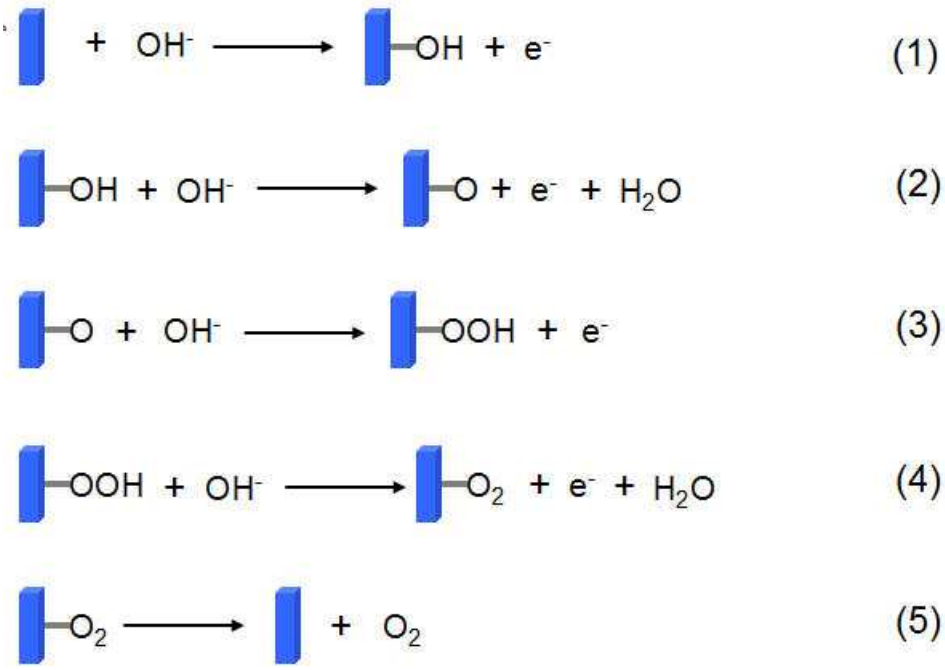

Figure S6. Schematic depiction of the mechanism for electrochemical oxygen evolution reaction on cobalt oxide. The blue box represents cobalt oxide. The Scheme is adapted from the work of Bell *et al.* for Au-supported cobalt oxide (**ref. S8**).

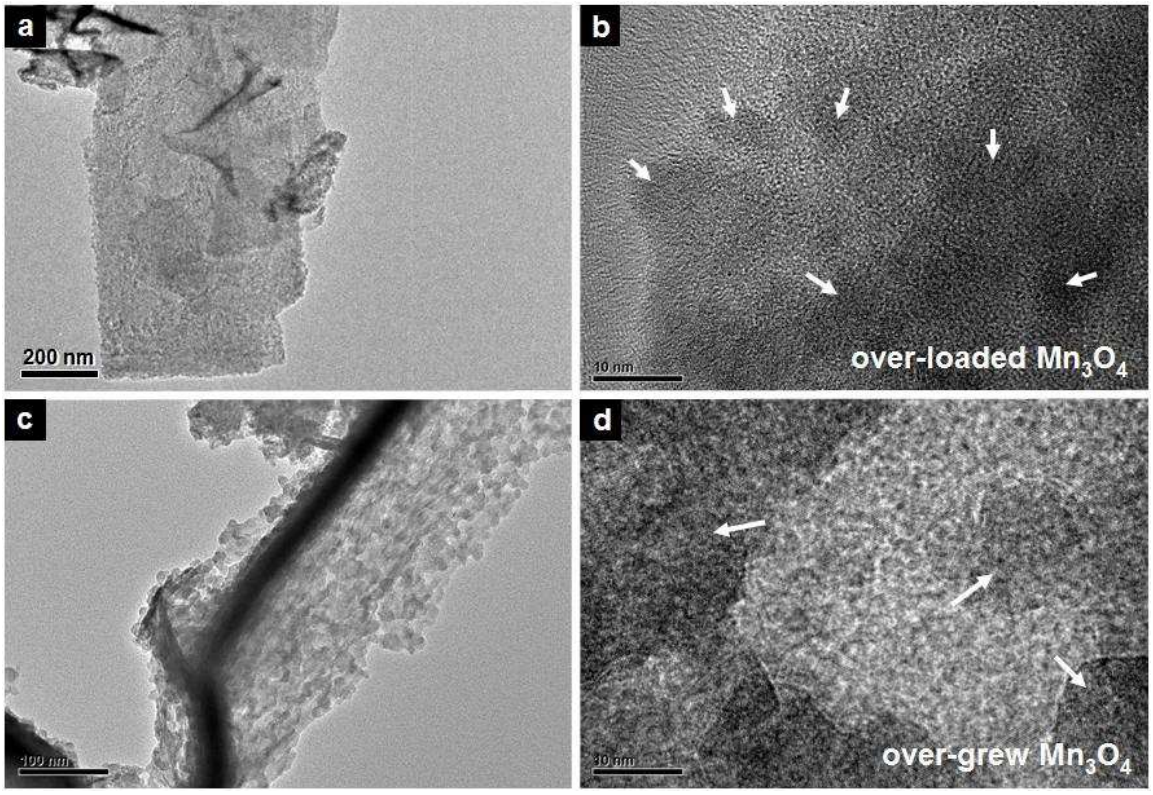

Figure S7. (a, b) TEM and HRTEM images of $Mn_3O_4/CoSe_2$ hybrid prepared at 278 ^oC for 1h with double $Mn(acac)_3$ feed, respectively. (c, d) TEM and HRTEM images of $Mn_3O_4/CoSe_2$ hybrid prepared at 290 ^oC for 1h, respectively.

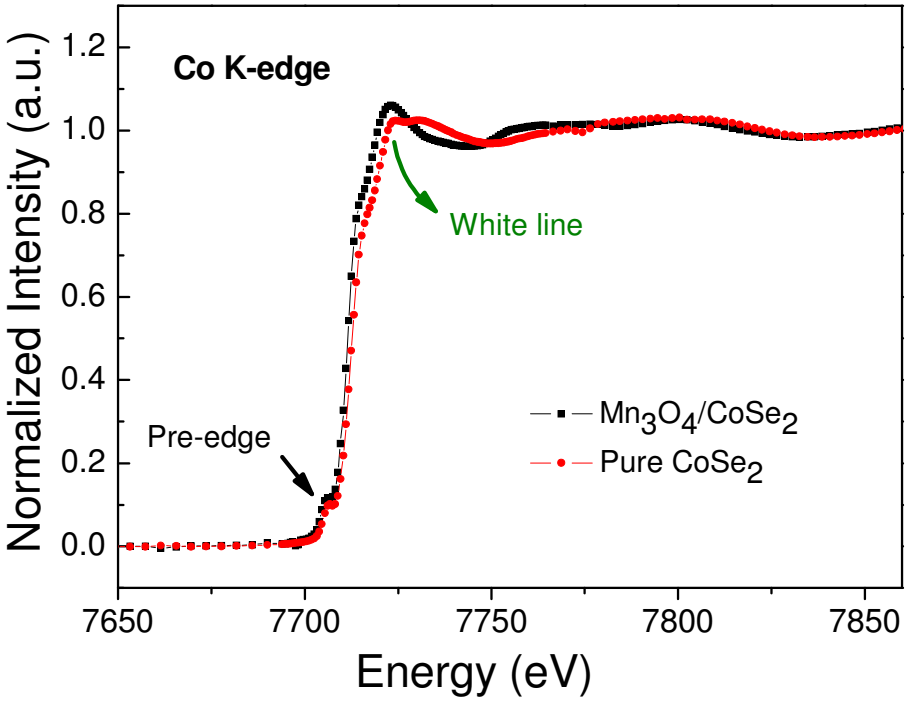

Figure S8. Co K-edge XANES spectra for pure $CoSe_2$/DETA NBs and as-constructed $Mn_3O_4/CoSe_2$ hybrid.

The normalized XANES spectra collected at Co K-edge measured at room temperature in the transmission mode at U7C XAFS station in NSRL. The deep analysis and interpretation of XANES spectra are complicate tasks that will not be addressed here. However, it is evident that the spectrum of pure $CoSe_2$/DETA is clearly different from that of $Mn_3O_4/CoSe_2$ hybrid. The change in the white line intensity in principle could be caused by the electronic effects (**ref. S9**). After loading $CoSe_2$ with Mn_3O_4 nanoparticles, the large increase in its white line intensity can be understood as being due to electron transfer from Mn_3O_4 to $CoSe_2$ support (**ref. S10**), which is in line with our XPS results.

Supporting Information Reference:

(Ref. S1) Gao, M. R.; Yao, W. T.; Yao, H. B.; Yu, S. H. *J. Am. Chem. Soc.* **2009**, 131, 7486.

(Ref. S2) Feng, Y. J.; He, T.; Alonso-Vante, N. *Chem. Mater.* **2008**, 20, 26.

(Ref. S3) Wang, H. L.; Liang, Y. Y.; Li, Y. G.; Dai, H. J. *Angew. Chem. Int. Ed.* **2011**, 50, 10969.

(Ref. S4) Gao, M. R.; Jiang, J.; Yu, S. H. *Small* **2011**, 7, DOI: 10.1002/small.201101573.

(Ref. S5) Gao, M. R.; Gao, Q.; Jiang, J.; Cui, C. H.; Yao, W. T.; Yu, S. H. *Angew. Chem. Int. Ed.* **2011**, 50, 4905.

(Ref. S6) Wang, N.; Guo, L.; He, L.; Cao, X.; Chen, C. P.; Wang, R. M.; Yang, S. H. *Small* **200**7, 3, 606.

(Ref. S7) Zhang, W. X.; Yang, Z. H.; Liu, Y.; Tang, S. P.; Han, X. Z.; Chen, M. *J. Cryst Growth* **2004**, 263, 394.

(Ref. S8) Yeo, B. S.; Bell, A. T. *J. Am. Chem. Soc.* **2011**, 133, 5587.

(**Ref. S9**) Brown, M.; Peierls, R. E.; Stern, E. A. *Phys. Rev. B* **1977**, 15, 738.

(**Ref. S10**) Ho, V. T. T.; Pan, C. J.; Rick, J.; Su, W. N.; Hwang, B. J. *J. Am. Chem. Soc.* **2011**, 133, 11716.